

Vanadium is an optimal element for strengthening in both fcc and bcc high-entropy alloys

Binglun Yin^{a,*}, Francesco Maresca^{a,b}, W. A. Curtin^a

^aLaboratory for Multiscale Mechanics Modeling (LAMMM) and National Centre for Computational Design and Discovery of Novel Materials (NCCR MARVEL), École Polytechnique Fédérale de Lausanne, 1015 Lausanne, Switzerland

^bEngineering and Technology Institute Groningen, Faculty of Science and Engineering, University of Groningen, 9747 AG, Netherlands

Abstract

The element Vanadium (V) appears unique among alloying elements for providing high strengthening in both the fcc Co-Cr-Fe-Mn-Ni-V and bcc Cr-Mo-Nb-Ta-V-W-Hf-Ti-Zr high-entropy alloy families. The origin of Vanadium's special role is its atomic volume: large in the fcc alloys and small in the bcc alloys, and thus having a large misfit volume in both crystalline structures. A parameter-free theory applicable to both fcc and bcc HEAs rationalizes this finding, with predictions of strength across a range of fcc and bcc alloys in quantitative and qualitative agreement with experiments. In the fcc class, the analysis demonstrates why the newly-discovered NiCoV and $\text{Ni}_{0.632}\text{V}_{0.368}$ alloys have far higher strength than any other fcc alloy and are predicted to be the highest attainable. In the bcc class, the analysis demonstrates that the addition of V always increases the strength relative to the same alloys without V. The optimization of complex alloys for high strength should thus center around the inclusion of V as a primary element at concentration levels of around 25 at. %

Keywords: high-entropy alloys, Vanadium, solute strengthening theory, yield strength

1. Introduction

High-entropy alloys (HEAs) are multicomponent alloys with high concentrations of all alloying elements. Alloys within this new class of structural metal alloys demonstrate impressive combinations of properties such as high strength and high fracture toughness [1, 2, 3, 4]. These attractive properties have driven an intense search for new alloys across the full range of number of components and composition. Designing new alloys or rationalizing alloy performance has, however, frequently relied on imprecise and non-quantitative concepts or correlations, such as “lattice distortions” [5, 6, 7, 8], electronegativity differences [9] and others [10]. With a vast composition space available for alloy design, physically-based and quantitatively-predictive theories are needed to guide the search for better-performing alloys while understanding the limits of performance. In fact, such theories have recently been developed for predicting alloy yield strength [11, 12] and have been shown to predict experiments across a range of HEA

systems. The success of these theories indicates that the solute misfit volumes are the dominant factor in strengthening. This insight points toward new promising alloy compositions in different alloy classes [13, 14, 12]. Theoretical results to date are on only a narrow range of alloys, and no fcc alloys containing Vanadium (V) have been studied. However, experimentally, alloys containing the element V provide the highest strengthening in both fcc and bcc alloys.

The primary experimental evidence for the role of V is revealed by examining two alloy families. In the fcc family of Co-Cr-Fe-Mn-Ni-V, the medium-entropy alloy NiCoV [5] and the binary alloy $\text{Ni}_{0.632}\text{V}_{0.368}$ [9] have recently been reported to have very high room temperature strengths as compared to all other alloys in this family. In the bcc refractory alloy family Mo-Nb-Ta-V-W, the MoNbTaVW has the highest retained strength at very high temperatures ($T > 1500$ K) [15, 16]. The fundamental origins of these extreme properties and their connections to the alloy composition were not previously established nor was the role of V as the critical element in both fcc and bcc recognized. Here, application of the new mechanistic models [11, 12] for strengthening in fcc and bcc HEAs explains the origin of V's

*Corresponding author

Email address: binglun.yin@epfl.ch (Binglun Yin)

45 potency for strengthening in HEAs. In particular, we
 46 make new quantitative predictions for the NiCoV and
 47 $\text{Ni}_{0.632}\text{V}_{0.368}$ fcc alloys in good agreement with experi-
 48 ments. These findings point toward future development
 49 of V-containing alloys as most promising for creating
 50 high strengths in both fcc and bcc alloys.

51 **High strength is not the sole requirement in alloy**
 52 **design. The high strength may compromise ductility,**
 53 **for instance. For V, the low melting point of Vana-**
 54 **dium oxide may limit the application of V-containing**
 55 **alloys to non-oxidizing situations. However, these is-**
 56 **ssues may also be overcome by tuning of other alloying**
 57 **elements or by engineering mitigation strategies such as**
 58 **protective coatings, enabling the exploitation of the high**
 59 **strength provided by V-containing alloys.**

60 2. Solute strengthening theory

61 The theoretical framework for understanding the spe-
 62 cial role of V is based on the fundamental interaction
 63 energy between a dislocation and the solutes that consti-
 64 tute the random alloy. In the random alloy, the random
 65 arrangement of solutes gives rise to spatially-fluctuating
 66 total interaction energies between the dislocation and
 67 the collective fluctuations in local solute concentrations.
 68 The dislocation becomes pinned in regions of favorable
 69 fluctuations, and this pinning is associated with high
 70 barriers for dislocation motion. These barriers are over-
 71 come only by high applied stresses and/or high temper-
 72 atures. A new general theory for the strength of random
 73 alloys based on the motion of edge dislocations through
 74 the random alloy, and encompassing both fcc and bcc
 75 crystal structures and for arbitrary number of compo-
 76 nents and arbitrary composition, embodies the physics
 77 of the problem [11, 12]. The full theory for the finite- T ,
 78 finite-strain-rate initial yield strength of an alloy can be
 79 reduced to an approximate analytical model under the
 80 assumption that the solute/dislocation interaction en-
 81 ergy U^n of a type- n solute is governed by elasticity the-
 82 ory, i.e., $U^n = -p\Delta V_n$, where ΔV_n is the misfit volume
 83 of the type- n solute ($n = 1, \dots, N$) in a N -component al-
 84 loy and p is the pressure field generated by the disloca-
 85 tion at the solute position. The theory then predicts the
 86 zero-temperature shear yield stress τ_{y0} and the energy
 87 barrier ΔE_b for thermally activated flow as

$$\begin{aligned} \tau_{y0} &= A_\tau \alpha^{-\frac{1}{3}} \mu_{\text{alloy}} \left[\frac{1 + \nu_{\text{alloy}}}{1 - \nu_{\text{alloy}}} \right]^{\frac{1}{3}} \left[\frac{\sum_n c_n \Delta V_n^2}{b^6} \right]^{\frac{2}{3}}, \\ \Delta E_b &= A_E \alpha^{\frac{1}{3}} \mu_{\text{alloy}} b^3 \left[\frac{1 + \nu_{\text{alloy}}}{1 - \nu_{\text{alloy}}} \right]^{\frac{1}{3}} \left[\frac{\sum_n c_n \Delta V_n^2}{b^6} \right]^{\frac{1}{3}}, \end{aligned} \quad (1)$$

88 At finite temperature T and finite strain rate $\dot{\epsilon}$, standard
 89 thermal activation theory then leads to the predicted ten-
 90 sile yield stress as

$$\sigma_y(T, \dot{\epsilon}) = 3.06 \tau_{y0} \left[1 - \left(\frac{kT}{\Delta E_b} \ln \frac{\dot{\epsilon}_0}{\dot{\epsilon}} \right)^{\frac{2}{3}} \right]. \quad (2)$$

91 Here, $\dot{\epsilon}_0 = 10^4 \text{ s}^{-1}$ is a reference strain rate and 3.06 is
 92 the Taylor factor for isotropic fcc and bcc polycrystals
 93 strengths controlled by edge dislocations. The quan-
 94 tities μ_{alloy} and ν_{alloy} are the shear modulus and Pois-
 95 son's ratio of the alloy and $\alpha = 0.125$ (fcc) or 0.0833
 96 (bcc) is related to the edge dislocation line tension as
 97 $\Gamma = \alpha \mu_{\text{alloy}} b^2$. For elastically anisotropic materials, the
 98 best estimates for μ_{alloy} and ν_{alloy} are the Voigt aver-
 99 ages [17], with the shear modulus in the line tension
 100 expression the value for the glide plane/direction of the
 101 dislocations. Often, however, only the isotropic poly-
 102 crystalline moduli are available from experiments which
 103 leads to some underestimate of the strength.

104 **The prefactor coefficients (A_τ , A_E) emerge from the**
 105 **reduced elasticity theory that depends only on the so-**
 106 **lute misfit volumes and the dislocation pressure field.**
 107 **These two material properties emerge as separated in**
 108 **the theory. The pressure field then depends only on**
 109 **the alloy elastic constants and dislocation core structure**
 110 **(distribution of Burgers vector), and so the coefficients**
 111 **(A_τ , A_E) depend only on these properties. Calculations**
 112 **[11, 12] of the typical atomistic structures of the (dis-**
 113 **sociated) fcc edge dislocation and the (undissociated)**
 114 **bcc edge dislocation lead to accurate alloy-independent**
 115 **prefactors (A_τ , A_E) = (0.01785, 1.5618) for fcc alloys**
 116 **and (A_τ , A_E) = (0.040, 2.00) for bcc alloys, reflecting**
 117 **the different atomic structures of fcc and bcc edge dis-**
 118 **locations. The details of full and reduced theory can be**
 119 **found in Ref. [11] for fcc alloys and Ref. [12] for bcc**
 120 **alloys.**

121 The theory demonstrates that the solute misfit vol-
 122 umes control strengthening because the alloy elastic
 123 moduli vary more slowly with composition. The mis-
 124 fit volumes ΔV_n of each type- n element ($n = 1, \dots, N$) in
 125 N -component random alloys at composition $\{c_n\}$ can be
 126 calculated as

$$\Delta V_n = \frac{\partial V_{\text{alloy}}}{\partial c_n} - \sum_{m=1}^N c_m \frac{\partial V_{\text{alloy}}}{\partial c_m}, \quad (3)$$

127 with alloy atomic volume $V_{\text{alloy}} = V_{\text{alloy}}(c_1, c_2, \dots, c_{N-1})$
 128 and $\partial V_{\text{alloy}} / \partial c_N = 0$ [18]. Therefore, the misfit volumes
 129 can be (i) measured experimentally [18], (ii) sometimes
 130 computed accurately by first-principles methods [14], or
 131 (iii) estimated. A widely-used approximation is Veg-

ard’s law $V_{\text{alloy}} = \sum_n c_n V_n$, leading to misfit volumes $\Delta V_n = V_n - V_{\text{alloy}}$ where V_n is the apparent volume of type- n element in the given crystal structure.

It is important to note several misconceptions related to the determination of misfit volumes that have arisen specifically in the study of V-containing alloys of interest here. First, the apparent volume of a solute is not the local Voronoi-volume around the solute in the lattice. The misfit volume involves distortions that extend to near-neighbor atoms and beyond, and the formal definition above (Eq. 3) encompasses all possible situations without the need to identify local atomic-scale details. Second, the misfit volume of a solute must be calculated in the alloy itself, or in an appropriate surrogate alloy having the same solute concentration. A misfit volume computed in a surrogate alloy in the dilute solute limit may be quite inaccurate because Vegard’s law does not always hold with sufficient accuracy. Below, we will show the errors caused by these estimates of misfit volume in the case of V.

With this broad background, we can now proceed to understand why the unique role of V for strengthening in both fcc and bcc HEAs is due to its atomic volume.

3. Results

3.1. Application of theory to fcc HEAs

We first consider the fcc Co-Cr-Fe-Mn-Ni-V family of HEAs, i.e., adding V to the well-established Cantor alloy family. We have computed the atomic volume of fcc V as 13.914 \AA^3 using first-principles spin-polarized DFT as implemented in VASP [19], where PBE [20] is used as the exchange-correlation functional and the PAW [21] pseudopotential includes V ($3s$, $3p$, $4s$, $3d$) as the valence states. (Detailed DFT parameters can be found in Ref. [14].) As shown in Table 1, this atomic volume is far larger than the apparent atomic volumes of the elements Ni, Co, Cr, Fe, and Mn as previously deduced from experiments on Ni, Ni-Co, Ni-Cr, and Ni-Fe binary alloys, and from Mn additions to various Co-Cr-Fe-Ni medium-entropy alloys [11]. To verify that the V atomic volume translates into a large misfit volume in Co-Cr-Fe-Mn-Ni-V alloys, we have also performed DFT calculations to compute the misfit volumes in random Ni_2V . In the DFT calculations, we compute the alloy atomic volumes of Ni-V alloys around the central composition, where c_{Ni} spans from 0.630 to 0.704. Then linear regression is performed to the DFT-computed alloy atomic volumes, which gives $V_{\text{alloy}} = 13.536 - 2.879c_{\text{Ni}}$ with $R^2 = 0.997$. This result then provides the DFT lattice constant of Ni_2V

($a = 3.595 \text{ \AA}$, $V_{\text{alloy}} = 11.617 \text{ \AA}^3$) and, more importantly, the misfit volumes $\Delta V_{\text{Ni}} = -0.960 \text{ \AA}^3$ and $\Delta V_{\text{V}} = 1.920 \text{ \AA}^3$. To remain consistent with the apparent volume of Ni (10.94 \AA^3), the corresponding apparent volume of V is determined as 13.8 \AA^3 , in good agreement with the elemental fcc V volume. Therefore, when V is added to alloys in the Cantor alloy family, the large misfit of V is predicted to generate a high strengthening relative to all other alloying elements in this family, in spite of the fact that V leads to a small reduction in elastic modulus.

Table 1: Apparent volumes of each element in fcc HEAs. The apparent volume of V is obtained from DFT calculations of fcc V and fcc Ni_2V . Other values were deduced from experiments on Ni, Ni-Co, Ni-Cr, and Ni-Fe binary alloys, and from Mn additions to various Co-Cr-Fe-Ni alloys.

	fcc apparent volumes V_n (\AA^3)
V	13.914 (from DFT of fcc V)
	13.8 (from DFT of Ni_2V , used in prediction)
Cr	12.27 ^a
Mn	12.60 ^a
Fe	12.09 ^a
Co	11.12 ^a
Ni	10.94 ^a

^a Ref. [11]. Varvenne et al., 2016.

Applying the incorrect Voronoi method to Ni_2V would yield an apparent V volume of 11.8 \AA^3 . This value is very close to the literature DFT Voronoi volume for NiCoV [5], but is, unfortunately, significantly smaller than the accurate value 13.8 \AA^3 derived here (Eq. 3). Other very recent literature [22] reports the apparent volume of V as 12.23 \AA^3 . However, this value was computed for V in Ni in the dilute limit (one V atom in a large cell). Our own calculations yielding 12.20 \AA^3 confirm this dilute-limit value, but it differs significantly from the value at more appropriate concentrations, e.g. 13.8 \AA^3 as computed here from Ni_2V .

Figure 1 shows the experimental and predicted strengths of various alloys in the Co-Cr-Ni-V sub-family. Comparisons are made after subtracting the so-called Hall-Petch grain-size-dependent strengthening to reveal only the intrinsic “chemical” strength predicted by the theory. We use the analytic model of Eqs. 1 and 2 with Vegard’s law, the atomic volumes in Table 1, and the experimental polycrystalline isotropic elastic constants. (See Appendix for detailed materials parameters.) NiCo has near-zero misfit and near-zero strength relative to pure Ni. Literature results on binary Ni-Cr at large grain size [23] lead to an estimated strength for Ni_2Cr of $\sim 150 \text{ MPa}$ while the theory predicts 144 MPa . NiCoCr has received considerable attention due to its high strength and exceptional fracture toughness among the Cantor alloy subsystems with equi-composition and

219 fcc single-phase. The experimental values from recent 246
 220 single crystal data [24], multiplied by 3.06 for compar- 247
 221 isons to polycrystal data, and various extrapolations 248
 222 from finite grain size polycrystalline data [18, 25] are 249
 223 in the range 150–210 MPa. The predicted strength using 250
 224 Eqs. 1 and 2 is 128 MPa but an improved prediction 251
 225 using anisotropic elasticity for this fairly anisotropic al- 252
 226 loy and the experimentally-measured misfit volumes in 253
 227 NiCoCr predicts 195 MPa [18].

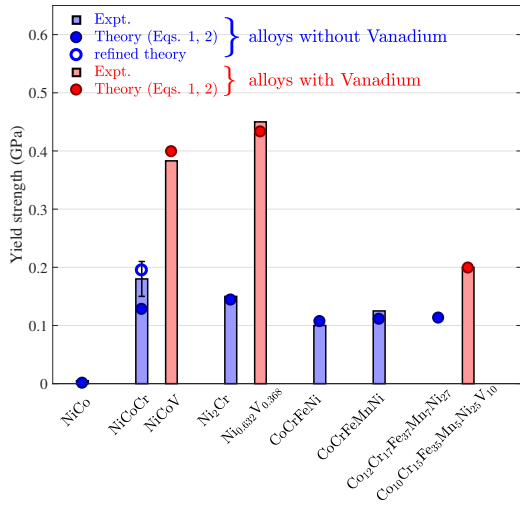


Figure 1: Yield strength of various fcc HEAs with (red) and with- 274
 275 out (blue) Vanadium, at room temperature and loading rate of 10^{-3} 276
 277 s^{-1} , as measured (bars) and as predicted (symbols) by the isotropic 278
 279 theory (Eq. 1 and 2). The atomic volume of V as determined from 280
 281 Ni₂V is used in all V-containing alloys. The refined theory prediction 282
 283 of NiCoCr is based on anisotropic elasticity and the experimentally 284
 285 measured misfit volumes.

228 Overwhelmingly stronger are the NiCoV [5] and 279
 229 Ni_{0.632}V_{0.368} [9] alloys recently been fabricated and 280
 230 tested. For NiCoV, we use the reported isotropic elas- 281
 231 tic constants $\mu = 72$ GPa, $\nu = 0.334$ and predict the 282
 232 yield stress at $T = 300$ K and $\dot{\epsilon} = 10^{-3} s^{-1}$ to be 399 283
 233 MPa. This is in excellent agreement with the experi- 284
 234 mental value of 383 MPa obtained by extrapolating fi- 285
 235 nite grain size data to infinite grain size. The theory 286
 236 then further indicates that the Ni-V binary alloys will be 287
 237 the strongest, because the binary uses only the small- 288
 238 est (Ni) and largest (V) elements. Because the predic- 289
 239 tion also depends on the dislocation Burgers vector 290
 240 $b = a/\sqrt{2}$ related to the alloy lattice constant a and 291
 241 the alloy elastic moduli, the optimal Ni-V binary al- 292
 242 loy favors compositions below the equi-composition al- 293
 243 loy. Using the theory of Eqs. 1 and 2, we predict the 294
 244 strength of Ni_{0.632}V_{0.368} to be 433 MPa. The reported 295
 245 yield strength of Ni_{0.632}V_{0.368} at grain size $8.1 \mu m$ is 750 296

MPa [9]. Using the Hall-Petch slope of NiCoV (864 246
 $MPa \cdot \mu m^{1/2}$) [5], the yield strength of Ni_{0.632}V_{0.368} at 247
 infinite grain size is estimated as ~ 450 MPa. This is 248
 again in good agreement with the theory. The theory 249
 predicts that no higher intrinsic yield strengths can be 250
 obtained across the entire family of Co-Cr-Fe-Mn-Ni-V 251
 alloys, and none have been reported to date. 252

To show the role of V more broadly, we ex- 253
 254 amine another V-containing alloy recently fabri- 255
 256 cated and tested [26]. The alloy composition is 257
 258 Co₁₀Cr₁₅Fe₃₅Mn₅Ni₂₅V₁₀, which is near the widely- 259
 260 studied equi-composition CoCrFeNi and Cantor alloys 261
 but with a relatively small addition of V. The yield 262
 strength for this alloy at a very small grain size of 5.2 263
 μm was measured to be 498 MPa. Extrapolating to infi- 264
 nite grain size using the average scaling for the closely- 265
 related CoCrFeNi ($860 MPa \cdot \mu m^{1/2}$) [27] and Cantor al- 266
 loy ($494 MPa \cdot \mu m^{1/2}$) [28] leads to an intrinsic strength 267
 of ~ 200 MPa. Application of the theory (Eq. 1 and 2) 268
 using the elastic moduli of the CoCrFeNi yields 199 269
 MPa, as shown in Fig. 1. We predict that the same al- 270
 loy without V, i.e., increasing all other components by 2 271
 at.% for a composition Co₁₂Cr₁₇Fe₃₇Mn₇Ni₂₇ and with 272
 no change in elastic constants, would have a strength 273
 of only 113 MPa. By extrapolating to the infinite 274
 grain size, the experimental yield strength for the V- 275
 free CoCrFeNi and Cantor alloys are also only ~ 100 276
 MPa [27] and ~ 125 MPa [28], respectively, with pre- 277
 dicted strengths of 107 MPa and 111 MPa (see Fig. 1). 278
 Thus, again, V addition, even at a smaller (but non- 279
 dilute) concentration of 10 at.%, provides a large (\sim 280
 76%) increase in strengthening relative to the V-free 281
 counterparts, and the theory predicts this strengthening. 282

3.2. Application of theory to bcc HEAs

Turning to the bcc alloys, the atomic volumes of the 283
 bcc elements Cr, Mo, Nb, Ta, V, W have been measured 284
 experimentally [29], as shown in Table 2. Experimen- 285
 tal studies of the lattice constants of various HEA alloys 286
 composed of these elements plus alloys containing Hf 287
 enable the estimation of Hf apparent volume based on 288
 Vegard’s law [30]. For Ti and Zr, which exist in the 289
 bcc structure only at high temperatures, extrapolations 290
 are carried out to estimate the apparent volumes at room 291
 temperature [31, 32]. Here, V stands out as the second- 292
 smallest element, with only Cr being smaller. However, 293
 Cr is smaller than V in both fcc and bcc and so although 294
 Cr can be potent for bcc alloys it is not nearly as effec- 295
 tive as V in fcc alloys (see Fig. 1). Furthermore, fabri- 296
 cation of single-phase random bcc alloys containing 297
 Cr can be challenging due to the strong tendency of Cr 298
 to form embrittling intermetallic compounds. Only V 299

297 is predicted to provide substantial strengthening in both
 298 fcc and bcc alloys.

Table 2: Apparent volumes of elements in bcc HEAs. The apparent volumes of Ti and Zr are obtained by extrapolation of high temperature bcc data to room temperature, and that for Hf is from Vegard’s law applied to experimental volumes of various Hf-containing HEAs. Other values are from the experimental lattice constants of the elements.

	bcc apparent volumes V_n (\AA^3)
Cr	12.321 ^a
V	14.020 ^a
Mo	15.524 ^a
W	15.807 ^a
Ti	17.387 ^b (high T extrapolated to RT)
Nb	17.952 ^a
Ta	17.985 ^a
Hf	22.528 ^c (from Vegard’s law on Hf-HEAs)
Zr	23.02 ^d (high T extrapolated to RT)

^a Ref. [29]. Simmons et al., 1971.

^b Ref. [31]. Petry et al., 1991.

^c Ref. [30]. Couzinie et al., 2015.

^d Ref. [32]. Heiming et al., 1991.

299 The role of V in bcc alloys is first revealed through
 300 a comparison of the refractory alloys MoNbTaW and
 301 MoNbTaVW, which differ only by the addition of V re-
 302 placing 5 at.% of each of the other 4 elements. The
 303 predictions of the theory and the experimental strengths
 304 versus temperature, as reported recently [12], are shown
 305 in Fig. 2. The V-containing alloy has a significantly
 306 higher strength over the entire temperature range. This
 307 is in spite of the fact that V has the lowest melting
 308 point of all of these elements, and elastic moduli that
 309 are $\sim 10\%$ lower than the 4-component alloy. The role
 310 of V is thus central to obtaining very high strength, as
 311 predicted. Many other bcc alloys in the Mo-Nb-Ta-V-W
 312 family also have high strengths, but there are no V-free
 313 counterparts in the literature; the theory predictions are
 314 consistent with these high strengths [12].

315 Examining other bcc alloy pairs where V is added,
 316 strengthening is found in all alloys. Figure 2 summa-
 317 rizes results reported in Miracle-Senkov [3], Couzinié-
 318 Miracle-Senkov-Dirrass [33], Senkov et al. [34], and
 319 Rao et al. [35]. In general, the predictions of the V-
 320 containing alloys are in good agreement ($\sim 15\%$) with
 321 the experiments. However, our predictions for the V-
 322 free alloys can be notably lower than experiments. One
 323 possible explanation is that there is a change from con-
 324 trol of the alloy strength by edge dislocations (with V)
 325 to screw dislocations (without V) in some alloys. In
 326 addition, our predictions for MoNbTaTiW both without
 327 and with V are lower than experiments. This could be
 328 attributed to the possible presence of high (1–2 at.%)
 329 interstitial Oxygen and/or Nitrogen content, which was

330 recently shown to increase strength by ~ 400 MPa at 2
 331 at.% interstitial O or N (and usually causing embrittle-
 332 ment, see [36]). The presence of O and N could be par-
 333 ticularly associated with the presence of Ti, consistent
 334 with experimental observations of increased strength
 335 upon Ti additions in some bcc alloys. Overall, in spite
 336 of some quantitative differences, all of the experimen-
 337 tal evidence on bcc alloys points to the role of V in
 338 achieving high strength, as compared to other alloy ad-
 339 ditions. Within the Mo-Nb-Ta-V-W family, the theo-
 340 ry further predicts that alloys $\text{Ta}_{0.33}\text{V}_{0.33+x}\text{W}_{0.33-x}$ with
 341 $-0.1 < x < 0.1$ will have the highest intrinsic strengths
 342 at high temperatures by taking advantage of both the
 343 large V misfit volume and the high stiffness of W. This
 344 prediction should drive experimental investigations of
 345 these alloys.

346 4. Conclusions

In summary, many new fcc and bcc high-entropy al-
 347 loys have been fabricated with V as one of many el-
 348 lements, and these alloys have high strengths relative
 349 to their counterparts without V. However, the critical
 350 role of V has not been recognized or understood. The
 351 centrality of solute misfit volumes, over all other ma-
 352 terial properties, is revealed through recent theory for
 353 strengthening in these complex random alloys. The
 354 uniqueness of V then follows from its atomic volume
 355 in fcc and bcc crystals: larger in fcc and smaller in bcc
 356 than other HEA alloying elements, creating large mis-
 357 fit volume and high strengthening in both fcc and bcc
 358 alloys. This singular feature of V makes it the prime
 359 element for use as a strengthener in both fcc and bcc
 360 HEAs, both as measured and as predicted by theory.
 361 **While strength is not the only application requirement,**
 362 **and the low-temperature formation of Vanadium oxide**
 363 **may limit applications of V-containing alloys in some**
 364 **situations,** the general insight revealed here, along with
 365 the theoretical models, can drive experimental alloy de-
 366 sign centered around V as a key elemental component.

368 Acknowledgments

This research was supported by the NCCR MAR-
 369 VEL, funded by the Swiss National Science Founda-
 370 tion. We also acknowledge support of high-
 371 performance computing provided by Scientific IT and
 372 Application Support (SCITAS) at EPFL.
 373

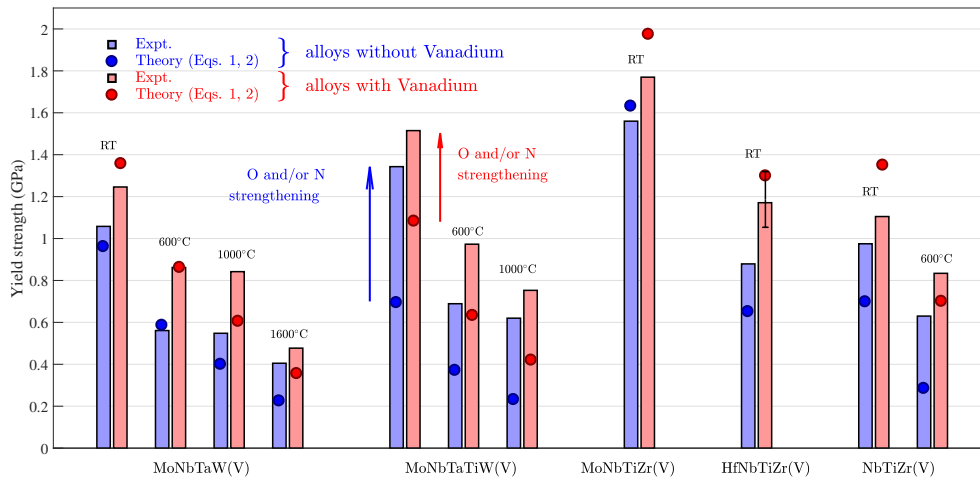


Figure 2: Yield strength of various bcc HEAs with (red) and without (blue) Vanadium, at various temperatures and loading rate of 10^{-3} s^{-1} (loading rate $0.2 \times 10^{-3} \text{ s}^{-1}$ for MoNbTiZr(V)), as measured (bars) and as predicted (symbols). Some Ti-containing alloys could be strengthened by O and/or N impurities at concentrations of 1–2 at.%, as indicated.

Appendix

For both fcc and bcc HEAs, the materials parameters that enter the solute strengthening model are summarized in Table 3. The resulting predictions are compared with the experimentally measured yield strength.

References

References

[1] E. P. George, D. Raabe, R. O. Ritchie, High-entropy alloys, *Nat. Rev. Mater.* 4 (2019) 515.
 [2] Y. Ikeda, B. Grabowski, F. Körmann, Ab initio phase stabilities and mechanical properties of multicomponent alloys: A comprehensive review for high entropy alloys and compositionally complex alloys, *Mater. Charact.* 147 (2019) 464–511.
 [3] D. B. Miracle, O. N. Senkov, A critical review of high entropy alloys and related concepts, *Acta Mater.* 122 (2017) 448–511.
 [4] B. Gludovatz, A. Hohenwarter, D. Catoor, E. H. Chang, E. P. George, R. O. Ritchie, A fracture-resistant high-entropy alloy for cryogenic applications, *Science* 345 (2014) 1153–1158.
 [5] S. S. Sohn, A. Kwiatkowski da Silva, Y. Ikeda, F. Körmann, W. Lu, W. S. Choi, B. Gault, D. Ponge, J. Neugebauer, D. Raabe, Ultrastrong Medium-Entropy Single-Phase Alloys Designed via Severe Lattice Distortion, *Adv. Mater.* 31 (2019) 1807142.
 [6] Z. Wang, Q. Fang, J. Li, B. Liu, Y. Liu, Effect of lattice distortion on solid solution strengthening of BCC high-entropy alloys, *J. Mater. Sci. Technol.* 34 (2018) 349–354.
 [7] H. Song, F. Tian, Q.-M. Hu, L. Vitos, Y. Wang, J. Shen, N. Chen, Local lattice distortion in high-entropy alloys, *Phys. Rev. Mater.* 1 (2017) 023404.
 [8] F. Körmann, M. H. Sluiter, Interplay between lattice distortions, vibrations and phase stability in NbMoTaW high entropy alloys, *Entropy* 18 (2016) 403.

[9] H. S. Oh, S. J. Kim, K. Odbadrakh, W. H. Ryu, K. N. Yoon, S. Mu, F. Körmann, Y. Ikeda, C. C. Tasan, D. Raabe, T. Egami, E. S. Park, Engineering atomic-level complexity in high-entropy and complex concentrated alloys, *Nat. Commun.* 10 (2019) 2090.
 [10] Y. Y. Zhao, Z. F. Lei, Z. P. Lu, J. C. Huang, T. G. Nieh, A simplified model connecting lattice distortion with friction stress of Nb-based equiatomic high-entropy alloys, *Mater. Res. Lett.* 7 (2019) 340–346.
 [11] C. Varvenne, A. Luque, W. A. Curtin, Theory of strengthening in fcc high entropy alloys, *Acta Mater.* 118 (2016) 164–176.
 [12] F. Maresca, W. A. Curtin, Mechanistic origin of high strength in refractory BCC high entropy alloys up to 1900K, *Acta Mater.* 182 (2020) 235–249.
 [13] C. Varvenne, W. A. Curtin, Predicting yield strengths of noble metal high entropy alloys, *Scr. Mater.* 142 (2018) 92–95.
 [14] B. Yin, W. A. Curtin, First-principles-based prediction of yield strength in the RhIrPdPtNiCu high-entropy alloy, *npj Comput. Mater.* 5 (2019) 14.
 [15] O. N. Senkov, G. B. Wilks, J. M. Scott, D. B. Miracle, Mechanical properties of Nb 25Mo 25Ta 25W 25 and V 20Nb 20Mo 20Ta 20W 20 refractory high entropy alloys, *Intermetallics* 19 (2011) 698–706.
 [16] S. Gorsse, D. B. Miracle, O. N. Senkov, Mapping the world of complex concentrated alloys, *Acta Mater.* 135 (2017) 177–187.
 [17] S. Nag, C. Varvenne, W. A. Curtin, Solute-strengthening in elastically anisotropic fcc alloys, *Model. Simul. Mater. Sci. Eng.* in press (2019).
 [18] B. Yin, S. Yoshida, N. Tsuji, W. A. Curtin, Yield strength and misfit volumes of NiCoCr and implications for short-range-order, submitted (2020).
 [19] G. Kresse, J. Furthmüller, Efficient iterative schemes for ab initio total-energy calculations using a plane-wave basis set, *Phys. Rev. B* 54 (1996) 11169–11186.
 [20] J. P. Perdew, K. Burke, M. Ernzerhof, Generalized Gradient Approximation Made Simple, *Phys. Rev. Lett.* 77 (1996) 3865–3868.

Table 3: Material parameters used in the solute strengthening model and the predicted strength (at $T = 300$ K and $\dot{\epsilon} = 10^{-3}$ s $^{-1}$) for various fcc and bcc HEAs. The lattice constant and δ -parameter are computed using Vegard’s law and the atom apparent volumes in Table 1 and 2. Here, $\delta = \sqrt{\sum_n c_n \Delta V_n^2} / (3V_{\text{alloy}})$ describes the collective effect of misfit volumes, with $V_{\text{alloy}} = a^3/4$ for fcc and $V_{\text{alloy}} = a^3/2$ for bcc. Some elastic moduli are assumed to be the same as similar systems due to the lack of literature data.

	a (Å)	δ (%)	μ (GPa)	ν	σ_y (MPa) (Theory)	σ_y (MPa) (Exp RT)
NiCo	3.534	0.272	84 ^a	0.26 ^a	1	$\sim 5^a$
NiCoCr	3.577	1.716	87 ^a	0.30 ^a	128	$\sim 150\text{--}210^d$
NiCoV	3.630	3.647	72 ^b	0.334 ^b	399	$\sim 383^b$
Ni ₂ Cr	3.571	1.836	87 (from NiCoCr)	0.30 (from NiCoCr)	144	$\sim 150^e$
Ni _{0.632} V _{0.368}	3.633	3.834	72 (from NiCoV)	0.334 (from NiCoV)	433	$\sim 450^f$
CoCrFeNi	3.594	1.672	84 ^a	0.28 ^a	107	$\sim 100^a$
CoCrFeMnNi	3.614	1.850	80 ^a	0.26 ^a	111	$\sim 125^a$
Co ₁₂ Cr ₁₇ Fe ₃₇ Mn ₇ Ni ₂₇	3.607	1.714	84 (from CoCrFeNi)	0.28 (from CoCrFeNi)	113	-
Co ₁₀ Cr ₁₅ Fe ₃₅ Mn ₅ Ni ₂₅ V ₁₀	3.627	2.353	84 (from CoCrFeNi)	0.28 (from CoCrFeNi)	199	$\sim 200^g$
MoNbTaW	3.228	2.291	103 ^h	0.31 ^h	954	$\sim 1058^i$
MoNbTaWV	3.192	3.124	92 ^h	0.32 ^h	1347	$\sim 1246^i$
MoNbTaTiW	3.235	2.084	87 ^h	0.32 ^h	688	$\sim 1343^j$
MoNbTaTiWV	3.204	2.945	81 ^h	0.32 ^h	1074	$\sim 1515^i$
MoNbTiZr	3.330	5.008	56 ^h	0.35 ^h	1661	$\sim 1560^i$
MoNbTiZrV	3.276	5.792	55 ^h	0.35 ^h	2008	$\sim 1770^i$
HfNbTiZr	3.432	4.227	29 ^h	0.39 ^h	643	$\sim 879^i$
HfNbTiZrV	3.361	5.932	34 ^h	0.38 ^h	1286	$\sim 1171^i$
NbTiZr	3.388	4.339	30 ^h	0.39 ^h	690	$\sim 975^j$
NbTiZrV	3.308	5.925	36 ^h	0.38 ^h	1337	$\sim 1105^i$

^a Ref. [11]. Varvenne et al., 2016.

^b Ref. [5]. Sohn et al., 2019.

^c Ref. [18]. Yin et al., 2019.

^d Ref. [18, 25].

^e Ref. [23]. Clement et al., 1984.

^f Ref. [9]. Oh et al., 2019.

^g Ref. [26]. Jo et al., 2017.

^h The anisotropic elastic constants C_{ij} of the alloy is estimated by applying “rule-of-mixtures” to the elemental C_{ij} , i.e., $C_{ij,\text{alloy}} = \sum_n c_n C_{ij,n}$. Then alloy isotropic elastic moduli are estimated (Bacon-Scattergood shear modulus $\mu = \sqrt{C_{44}(C_{11} - C_{12})/2}$, bulk modulus $B = (C_{11} + 2C_{12})/3$, Poisson’s ratio $\nu = \nu(\mu, B)$).

ⁱ Ref. [33]. Couzinie et al., 2018.

^j Ref. [34]. Senkov et al., 2018.

- 442 [21] G. Kresse, D. Joubert, From ultrasoft pseudopotentials to the
443 projector augmented-wave method, *Phys. Rev. B* 59 (1999)
444 1758–1775.
- 445 [22] D. Wen, C.-H. Chang, S. Matsunaga, G. Park, L. Ecker, S. K.
446 Gill, M. Topsakal, M. A. Okuniewski, S. Antonov, D. R.
447 Johnson, M. S. Titus, Structure and Tensile Properties of
448 $Mx(MnFeCoNi)_{100-x}$ Solid Solution Strengthened High En-
449 tropy Alloys, *Materialia* 9 (2020) 100539.
- 450 [23] N. Clément, D. Caillard, J. L. Martin, Heterogeneous defor-
451 mation of concentrated NiCr F.C.C. alloys: Macroscopic and
452 microscopic behaviour, *Acta Metall.* 32 (1984) 961–975.
- 453 [24] B. Uzer, S. Picak, J. Liu, T. Jozaghi, D. Canadinc, I. Karaman,
454 Y. I. Chumlyakov, I. Kireeva, On the mechanical response and
455 microstructure evolution of NiCoCr single crystalline medium
456 entropy alloys, *Mater. Res. Lett.* 6 (2018) 442–449.
- 457 [25] M. Schneider, E. P. George, T. J. Manescau, T. Zálezák, J. Hun-
458 feld, A. Dlouhý, G. Eggeler, G. Laplanche, Analysis of strength-
459 ening due to grain boundaries and annealing twin boundaries in
460 the CrCoNi medium-entropy alloy, *Int. J. Plast.* 124 (2020) 155–
461 169.
- 462 [26] Y. H. Jo, S. Jung, W. M. Choi, S. S. Sohn, H. S. Kim, B. J.
463 Lee, N. J. Kim, S. Lee, Cryogenic strength improvement by uti-
464 lizing room-temperature deformation twinning in a partially re-
465 crystallized VCrMnFeCoNi high-entropy alloy, *Nat. Commun.*
466 8 (2017) 1–8.
- 467 [27] Z. Wu, H. Bei, G. M. Pharr, E. P. George, Temperature depen-
468 dence of the mechanical properties of equiatomic solid solution
469 alloys with face-centered cubic crystal structures, *Acta Mater.*
470 81 (2014) 428–441.
- 471 [28] F. Otto, A. Dlouhý, C. Somsen, H. Bei, G. Eggeler, E. P. George,
472 The influences of temperature and microstructure on the tensile
473 properties of a CoCrFeMnNi high-entropy alloy, *Acta Mater.*
474 61 (2013) 5743–5755.
- 475 [29] G. Simmons, H. Wang, Single crystal elastic constants and
476 calculated aggregate properties: a handbook, The M.I.T.
477 Press, 1971. URL: https://books.google.ch/books?id=bPwtz_JztBEC.
- 478 [30] J. P. Couzinié, L. Lilensten, Y. Champion, G. Dirras, L. Perrière,
479 I. Guillot, On the room temperature deformation mechanisms of
480 a TiZrHfNbTa refractory high-entropy alloy, *Mater. Sci. Eng. A*
481 645 (2015) 255–263.
- 482 [31] W. Petry, A. Heiming, J. Trampenau, M. Alba, C. Herzig, H. R.
483 Schober, G. Vogl, Phonon dispersion of the bcc phase of group-
484 IV metals. I. bcc titanium, *Phys. Rev. B* 43 (1991) 10933.
- 485 [32] A. Heiming, W. Petry, J. Trampenau, M. Alba, C. Herzig, H. R.
486 Schober, G. Vogl, Phonon dispersion of the bcc phase of group-
487 IV metals. II. bcc zirconium, a model case of dynamical precu-
488 sors of martensitic transitions, *Phys. Rev. B* 43 (1991) 10948.
- 489 [33] J. P. Couzinié, O. N. Senkov, D. B. Miracle, G. Dirras, Com-
490 prehensive data compilation on the mechanical properties of re-
491 fractory high-entropy alloys, *Data Br.* 21 (2018) 1622–1641.
- 492 [34] O. N. Senkov, S. Rao, K. J. Chaput, C. Woodward, Composi-
493 tional effect on microstructure and properties of NbTiZr-based
494 complex concentrated alloys, *Acta Mater.* 151 (2018) 201–215.
- 495 [35] S. I. Rao, B. Akdim, E. Antillon, C. Woodward, T. A.
496 Parthasarathy, O. N. Senkov, Modeling solution hardening in
497 BCC refractory complex concentrated alloys: NbTiZr, Nb 1.5
498 TiZr 0.5 and Nb 0.5 TiZr 1.5, *Acta Mater.* 168 (2019) 222–236.
- 499 [36] Z. Lei, X. Liu, Y. Wu, H. Wang, S. Jiang, S. Wang, X. Hui,
500 Y. Wu, B. Gault, P. Kontis, D. Raabe, L. Gu, Q. Zhang, H. Chen,
501 H. Wang, J. Liu, K. An, Q. Zeng, T. G. Nieh, Z. Lu, Enhanced
502 strength and ductility in a high-entropy alloy via ordered oxygen
503 complexes, *Nature* 563 (2018) 546–550.